Frontiers of Information Technology & Electronic Engineering
www.jzus.zju.edu.cn; engineering.cae.cn; www.springerlink.com
ISSN 2095-9184 (print); ISSN 2095-9230 (online)
E-mail: jzus@zju.edu.cn

An improved subspace weighting method using random matrix theory*

Yu-meng GAO[1], Jiang-hui LI[2], Ye-chao BAI[†‡1], Qiong WANG[1], Xing-gan ZHANG[1]

[1]*School of Electronic Science and Engineering, Nanjing University, Nanjing 210023, China*

[2]*Institute of Sound and Vibration Research, University of Southampton, Southampton SO17 1BJ, UK*

[†]E-mail: ychbai@nju.edu.cn

Received Sept. 2, 2019; Revision accepted Dec. 30, 2019; Crosschecked Aug. 10, 2020

Abstract: The weighting subspace fitting (WSF) algorithm performs better than the multi-signal classification (MUSIC) algorithm in the case of low signal-to-noise ratio (SNR) and when signals are correlated. In this study, we use the random matrix theory (RMT) to improve WSF. RMT focuses on the asymptotic behavior of eigenvalues and eigenvectors of random matrices with dimensions of matrices increasing at the same rate. The approximative first-order perturbation is applied in WSF when calculating statistics of the eigenvectors of sample covariance. Using the asymptotic results of the norm of the projection from the sample covariance matrix signal subspace onto the real signal in the random matrix theory, the method of calculating WSF is obtained. Numerical results are shown to prove the superiority of RMT in scenarios with few snapshots and a low SNR.

Key words: Direction of arrival; Signal subspace; Random matrix theory
https://doi.org/10.1631/FITEE.1900463 **CLC number:** TP319

1 Introduction

Estimation of the direction of arrival (DOA) of narrow-band signals in array signals has been widely studied (Krim and Viberg, 1996; Zhao et al., 2015). Schmidt (1986) first proposed the multi-signal classification (MUSIC) algorithm, which starts the research of subspace algorithms in array signal processing. Algorithms of MUSIC (Basha et al., 2013) and root MUSIC (Li et al., 2014; Liu et al., 2018) directly give solutions of the parameter estimate and avoid spectral peak search in MUSIC. The process of calculating the weighting matrix is given in the weighting subspace fitting (WSF) method (Viberg et al., 1991; Bai XJ et al., 2014), and the estimation error (Wu and Guo, 2011) of WSF is significantly lower than the error produced by MUSIC with a small number of snapshots and a low signal-to-noise ratio (SNR). Random matrix theory (RMT) (Bai YC et al., 2018; Chen et al., 2018) concentrates on studying the asymptotic behavior of eigenvalues and eigenvectors of random matrices when the dimensions of matrices increase at the same rate, making RMT-based algorithms suitable for scenarios with a small number of snapshots and a low SNR. The RMT-based method proposed here, however, is targeting to obtain better performance.

2 Proposed method

Considering a linear array (Wan et al., 2017) with M sensors receiving N narrow-band signals from the far field, the M-dimensional output $\boldsymbol{x}$ of the array is modeled as

$$\boldsymbol{x} = \boldsymbol{A}(\boldsymbol{\theta})\boldsymbol{s} + \boldsymbol{n}, \tag{1}$$

‡ Corresponding author

* Project supported by the National Natural Science Foundation of China (No. 61976113)

ORCID: Yu-meng GAO, https://orcid.org/0000-0002-3053-2775; Ye-chao BAI, https://orcid.org/0000-0001-5244-674X

where $\boldsymbol{A}(\boldsymbol{\theta})=[\boldsymbol{a}(\theta_1),\ \boldsymbol{a}(\theta_2),\ \ldots,\ \boldsymbol{a}(\theta_N)]$ denotes the $M\times N$ steering matrix with θ_i being the DOA of the i^{th} signal for $i=1,\ 2,\ \ldots,\ N$. The N-dimensional source signal $\boldsymbol{s}$ is assumed to be Gaussian distributed with zero mean, and the M-dimensional $\boldsymbol{n}$ is the additive zero-mean Gaussian noise. The eigen structure of array covariance $\boldsymbol{R}$ can be written as

$$\boldsymbol{R}=\boldsymbol{U}_{\mathrm{s}}\boldsymbol{\Lambda}_{\mathrm{s}}\boldsymbol{U}_{\mathrm{s}}^{\mathrm{H}}+\sigma^2\boldsymbol{U}_{\mathrm{n}}\boldsymbol{U}_{\mathrm{n}}^{\mathrm{H}}, \tag{2}$$

where $(\cdot)^{\mathrm{H}}$ denotes the conjugate transpose, $\boldsymbol{U}_{\mathrm{s}}$ is called the signal subspace, and its eigenvectors $\boldsymbol{u}_i$ correspond to the largest N eigenvalues in descending order in the diagonal matrix $\boldsymbol{\Lambda}_{\mathrm{s}}=\mathrm{diag}(\sigma_1^2,\ \sigma_2^2,\ \ldots,\ \sigma_N^2)$. The noise subspace spanned by $\boldsymbol{U}_{\mathrm{n}}$ contains $(M-N)$ eigenvectors corresponding to the eigenvalue σ^2, which is also the variance of noise $\boldsymbol{n}$. Normally, $\boldsymbol{R}$ is obtained through the sample covariance $\hat{\boldsymbol{R}}$, which is calculated as

$$\hat{\boldsymbol{R}}=\frac{1}{L}\sum_{t=1}^{L}\boldsymbol{x}(t)\boldsymbol{x}^{\mathrm{H}}(t), \tag{3}$$

where L is the number of snapshots.

As $M,\ L\to\infty$ and $M/L\to c\in(0,\infty)$, the equation below is obtained from RMT (Benaych-Georges and Nadakuditi, 2011; Asendorf, 2015):

$$\begin{aligned}\hat{\boldsymbol{U}}_{\mathrm{s}}^{\mathrm{H}}\boldsymbol{U}_{\mathrm{s}}\boldsymbol{U}_{\mathrm{s}}^{\mathrm{H}}\hat{\boldsymbol{U}}_{\mathrm{s}}&\overset{\text{a.s.}}{\to}\mathrm{diag}\left(|\langle\boldsymbol{u}_1,\ \hat{\boldsymbol{u}}_1\rangle|^2,\right.\\&\left.|\langle\boldsymbol{u}_2,\ \hat{\boldsymbol{u}}_2\rangle|^2,\ \ldots,\ |\langle\boldsymbol{u}_N,\ \hat{\boldsymbol{u}}_N\rangle|^2\right),\end{aligned} \tag{4}$$

where $\hat{\boldsymbol{U}}_{\mathrm{s}}$ and $\hat{\boldsymbol{u}}_i$ are the estimates of $\boldsymbol{U}_{\mathrm{s}}$ and $\boldsymbol{u}_i$, respectively. $\hat{\boldsymbol{U}}_{\mathrm{s}}$ contains N eigenvectors corresponding to the largest N eigenvalues of $\hat{\boldsymbol{R}}$, $\overset{\text{a.s.}}{\to}$ denotes almost sure convergence, and $|\langle\boldsymbol{u}_i,\ \hat{\boldsymbol{u}}_i\rangle|^2$ is expressed by

$$\begin{aligned}&|\langle\boldsymbol{u}_i,\ \hat{\boldsymbol{u}}_i\rangle|^2\\&\overset{\text{a.s.}}{\to}\alpha_i^2=\begin{cases}1-\dfrac{c\,(1+\lambda_i)}{\lambda_i\,(\lambda_i+c)}, & \lambda_i>c^{1/2},\\ 0, & \text{otherwise},\end{cases}\end{aligned} \tag{5}$$

where λ_i is calculated by $\left(\hat{\sigma}_i^2-\hat{\sigma}^2\right)/\hat{\sigma}^2$. $\hat{\sigma}_i^2$ are the largest N eigenvalues of the sample covariance matrix $\hat{\boldsymbol{R}}$, and $\hat{\sigma}^2$ is calculated by averaging the smallest $(M-N)$ eigenvalues of $\hat{\boldsymbol{R}}$. In theory, we require that M and L are infinite, which is infeasible in the practical world. The results, however, are remarkably accurate, even for relatively moderate M and L such as tens (He et al., 2017). Our simulation can also prove its accuracy when the number of snapshots is close to 12.

The convergence of $\hat{\boldsymbol{U}}_{\mathrm{s}}^{\mathrm{H}}\boldsymbol{U}_{\mathrm{s}}\boldsymbol{U}_{\mathrm{s}}^{\mathrm{H}}\hat{\boldsymbol{U}}_{\mathrm{s}}$ is demonstrated in Fig. 1, where M/L was set as 1. When there are only a few snapshots, the diagonal values of $\hat{\boldsymbol{U}}_{\mathrm{s}}^{\mathrm{H}}\boldsymbol{U}_{\mathrm{s}}\boldsymbol{U}_{\mathrm{s}}^{\mathrm{H}}\hat{\boldsymbol{U}}_{\mathrm{s}}$ are close to α_i^2; as shown in Fig. 1a, the diagonal value is the second one and $i=2$. The non-diagonal values are almost equivalent to 0; as shown in Fig. 1b, the non-diagonal item is in row 2, column 1, which also proves the validity of Eqs. (4) and (5).

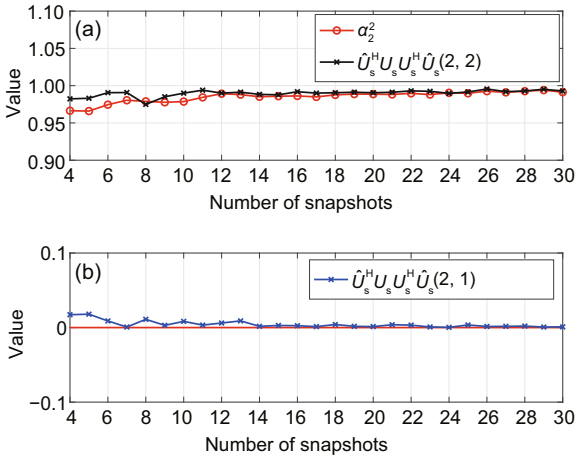

Fig. 1 Convergence of $\hat{\boldsymbol{U}}_{\mathrm{s}}^{\mathrm{H}}\boldsymbol{U}_{\mathrm{s}}\boldsymbol{U}_{\mathrm{s}}^{\mathrm{H}}\hat{\boldsymbol{U}}_{\mathrm{s}}$ ($M/L=1$; SNR= −3 dB; number of snapshots: 4–30): (a) the second diagonal value of $\hat{\boldsymbol{U}}_{\mathrm{s}}^{\mathrm{H}}\boldsymbol{U}_{\mathrm{s}}\boldsymbol{U}_{\mathrm{s}}^{\mathrm{H}}\hat{\boldsymbol{U}}_{\mathrm{s}}$ converges to α_2^2; (b) the non-diagonal value of $\hat{\boldsymbol{U}}_{\mathrm{s}}^{\mathrm{H}}\boldsymbol{U}_{\mathrm{s}}\boldsymbol{U}_{\mathrm{s}}^{\mathrm{H}}\hat{\boldsymbol{U}}_{\mathrm{s}}$ at row 2, column 1 converges to 0

From

$$\hat{\boldsymbol{U}}_{\mathrm{s}}^{\mathrm{H}}\boldsymbol{U}_{\mathrm{n}}\boldsymbol{U}_{\mathrm{n}}^{\mathrm{H}}\hat{\boldsymbol{U}}_{\mathrm{s}}+\hat{\boldsymbol{U}}_{\mathrm{s}}^{\mathrm{H}}\boldsymbol{U}_{\mathrm{s}}\boldsymbol{U}_{\mathrm{s}}^{\mathrm{H}}\hat{\boldsymbol{U}}_{\mathrm{s}}=\boldsymbol{I}, \tag{6}$$

we have

$$\hat{\boldsymbol{U}}_{\mathrm{s}}^{\mathrm{H}}\boldsymbol{U}_{\mathrm{n}}\boldsymbol{U}_{\mathrm{n}}^{\mathrm{H}}\hat{\boldsymbol{U}}_{\mathrm{s}}\overset{\text{a.s.}}{\to}\mathrm{diag}\left(1-\alpha_1^2,\ 1-\alpha_2^2,\ \ldots,\ 1-\alpha_N^2\right). \tag{7}$$

A certain column of $\hat{\boldsymbol{U}}_{\mathrm{s}}$ is $\hat{\boldsymbol{u}}_i$, which is Gaussian independent and identically distributed (IID) (Viberg et al., 1991). Let $\hat{\boldsymbol{c}}_i(\boldsymbol{\theta})=\boldsymbol{U}_{\mathrm{n}}^{\mathrm{H}}\hat{\boldsymbol{u}}_i$; for simplicity, $\hat{\boldsymbol{c}}_i(\boldsymbol{\theta})$ will be denoted as $\hat{\boldsymbol{c}}_i$ in the following. Then $\hat{\boldsymbol{c}}_i^{\mathrm{H}}\hat{\boldsymbol{c}}_i\approx 1-\alpha_i^2$. $\hat{\boldsymbol{c}}_i$ is also Gaussian IID; thus, the mean and variance are easily given by

$$E\left(\hat{\boldsymbol{c}}_i\right)\approx\boldsymbol{0}, \tag{8}$$

$$E\left(\hat{\boldsymbol{c}}_i\hat{\boldsymbol{c}}_i^{\mathrm{H}}\right)\approx\frac{1-\alpha_i^2}{M-N}\boldsymbol{I}_{M-N}. \tag{9}$$

The log likelihood function $l(\hat{\boldsymbol{c}}_1,\ \hat{\boldsymbol{c}}_2,\ \ldots,\ \hat{\boldsymbol{c}}_N|\boldsymbol{\theta})$ is

$$\begin{aligned} &l(\hat{\boldsymbol{c}}_1,\ \hat{\boldsymbol{c}}_2,\ \ldots,\ \hat{\boldsymbol{c}}_N|\boldsymbol{\theta})\\ =&-\sum_{i=1}^{N}\log\left((2\pi)^{(M-N)/2}(1-\alpha_i^2)\right)\\ &-\frac{1}{2}\sum_{i=1}^{N}\hat{\boldsymbol{c}}_i^{\mathrm{H}}\left(\frac{1-\alpha_i^2}{M-N}\right)^{-1}\hat{\boldsymbol{c}}_i. \end{aligned} \tag{10}$$

The maximum of the log likelihood function that obtains the argument $\boldsymbol{\theta}$ can be written as

$$\begin{aligned} &\max_{\boldsymbol{\theta}} l(\hat{\boldsymbol{c}}_1,\ \hat{\boldsymbol{c}}_2,\ \ldots,\ \hat{\boldsymbol{c}}_N|\boldsymbol{\theta})\\ =&\min_{\boldsymbol{\theta}}\sum_{i=1}^{N}\hat{\boldsymbol{c}}_i^{\mathrm{H}}\left(\frac{1-\alpha_i^2}{M-N}\right)^{-1}\hat{\boldsymbol{c}}_i\\ =&\min_{\boldsymbol{\theta}}\operatorname{tr}\left(\sum_{i=1}^{N}w_i\hat{\boldsymbol{c}}_i\hat{\boldsymbol{c}}_i^{\mathrm{H}}\right)\\ =&\min_{\boldsymbol{\theta}}\operatorname{tr}\left\{\boldsymbol{P}_A^{\perp}\hat{\boldsymbol{U}}_{\mathrm{s}}\boldsymbol{W}_{\mathrm{RMT}}\hat{\boldsymbol{U}}_{\mathrm{s}}^{\mathrm{H}}\right\}\\ =&\max_{\boldsymbol{\theta}}\operatorname{tr}\left\{\boldsymbol{P}_A\hat{\boldsymbol{U}}_{\mathrm{s}}\boldsymbol{W}_{\mathrm{RMT}}\hat{\boldsymbol{U}}_{\mathrm{s}}^{\mathrm{H}}\right\}, \end{aligned} \tag{11}$$

where

$$\begin{cases} \boldsymbol{P}_A^{\perp}=\boldsymbol{U}_{\mathrm{n}}\boldsymbol{U}_{\mathrm{n}}^{\mathrm{H}},\\ \boldsymbol{P}_A=\boldsymbol{I}-\boldsymbol{P}_A^{\perp}=\boldsymbol{A}(\boldsymbol{A}^{\mathrm{H}}\boldsymbol{A})^{-1}\boldsymbol{A}^{\mathrm{H}},\\ w_i=1/(1-\alpha_i^2). \end{cases}$$

Then the weighting matrix is

$$\begin{aligned} \boldsymbol{W}_{\mathrm{RMT}}&=\operatorname{diag}(w_1,\ w_2,\ \ldots,\ w_N)\\ &=\operatorname{diag}\left(\frac{1}{1-\alpha_1^2},\ \frac{1}{1-\alpha_2^2},\ \ldots,\ \frac{1}{1-\alpha_N^2}\right). \end{aligned} \tag{12}$$

Note that the weighting coefficient in Eq. (12) is formally similar to that for the multi-frequency spatial spectrum in Bai YC et al. (2018); however, it is used under the single-frequency multi-signal subspace. Furthermore, the two methods have different calculations of α.

The weighting matrix in WSF (Viberg et al., 1991) can be calculated by

$$\begin{aligned} \boldsymbol{W}_{\mathrm{WSF}}=&\operatorname{diag}\left(\frac{(\hat{\sigma}_1^2-\hat{\sigma}^2)^2}{\hat{\sigma}^2},\ \frac{(\hat{\sigma}_2^2-\hat{\sigma}^2)^2}{\hat{\sigma}^2},\right.\\ &\left.\ldots,\ \frac{(\hat{\sigma}_N^2-\hat{\sigma}^2)^2}{\hat{\sigma}^2}\right). \end{aligned} \tag{13}$$

Because of the complex computation of multi-dimensional search, one-dimensional search with corresponding degrees of the largest N peaks of the expression is the result of the estimation of DOA. It is applied to simplify operations to estimate directions; i.e., $\boldsymbol{A}$ is replaced by $\boldsymbol{a}$. In practice, optimization of the problem of the last expression in Eq. (11), therefore, can be simplified as

$$\begin{aligned} &\max_{\boldsymbol{\theta}}\operatorname{tr}\left\{\boldsymbol{a}(\boldsymbol{a}^{\mathrm{H}}\boldsymbol{a})^{-1}\boldsymbol{a}^{\mathrm{H}}\hat{\boldsymbol{U}}_{\mathrm{s}}\boldsymbol{W}_{\mathrm{RMT}}\hat{\boldsymbol{U}}_{\mathrm{s}}^{\mathrm{H}}\right\}\\ =&\max_{\boldsymbol{\theta}}\operatorname{tr}\left\{\boldsymbol{a}\hat{\boldsymbol{U}}_{\mathrm{s}}\boldsymbol{W}_{\mathrm{RMT}}\hat{\boldsymbol{U}}^{\mathrm{H}}\boldsymbol{a}^{\mathrm{H}}\right\}. \end{aligned} \tag{14}$$

3 Simulation results

In this section, simulations are performed to verify the superiority of the proposed method. We assume that three signals located at 10°, 40°, and 60° respectively are received by a linear array with 15 sensors and generated by three zero-mean Gaussian random variables with variances determined by SNR. The variance of noise is set as 1. Our simulations are performed under three different scenarios. First, the number of snapshots is fixed at 10 with SNR ranging from −10 to −2 dB. The first and second variables are correlated with a correlation coefficient of 0.8, and the third variable is uncorrelated to the first two. Second, SNR is fixed at −3 dB with the number of snapshots set from 4 to 18, and the three signals are the same as those in the first scenario. In the third scenario, the simulation is performed with three uncorrelated signals when the number of snapshots is set at 10 with SNR varying from −14 to −8 dB.

The performances of the MUSIC method, spatial smoothing method (SSP), compressive sensing (CS), WSF method, and the proposed method (RMT) are compared. The root mean square error (RMSE) of each algorithm in each simulation is averaged over 10 000 trials with independent signals and noise realizations. RMSE can be calculated by

$$\mathrm{RMSE}=\sqrt{\frac{1}{Y}\frac{1}{N}\sum_{y=1}^{Y}\sum_{i=1}^{N}\left(\hat{\theta}_i^y-\theta_i\right)^2}, \tag{15}$$

where Y is the number of trials and $\hat{\theta}_i^y$ is an estimate of θ_i in the y^{th} trial.

Fig. 2 shows the normalized amplitudes of spatial spectrum of MUSIC, SSP, CS, WSF, and RMT versus the search direction ranging from –90° to 90°,

with the DOAs at 10°, 40°, and 60°. The corresponding angles of the three largest peaks of RMT are all around the given DOAs, and are high enough to distinguish easily. The curve of WSF basically coincides with that of RMT, but the peaks of WSF around 10° and 40° are slightly lower than those of RMT. The spike of CS around 40° has a larger error than those around 10° and 60°. The peaks of SSP around 10° and 60° are sharper than that around 40°, and the position of the peak around 40° has a larger deviation. The spikes of MUSIC around DOA exist, but there might still be large spikes at other locations that may easily be misjudged as targets at a low SNR.

In Fig. 3, the estimation errors of MUSIC, SSP, CS, WSF, and RMT are plotted under the first scenario. Fig. 4 shows the estimation error curves of the five methods under the second scenario. As shown in Figs. 3 and 4, when the SNR and number of snapshots are less than −2 dB and 16 respectively, the performance of the RMT method is superior to those of the others. While the SNR and the number of snapshots are comparatively large, all five methods achieve better performance, and estimation errors almost converge to the same value as SNR and the number of snapshots increase.

Figs. 5 and 6 show the probability of outliers of MUSIC, SSP, CS, WSF, and RMT under the first and second scenarios, respectively. In our simulation, the estimated angles deviating from the true ones

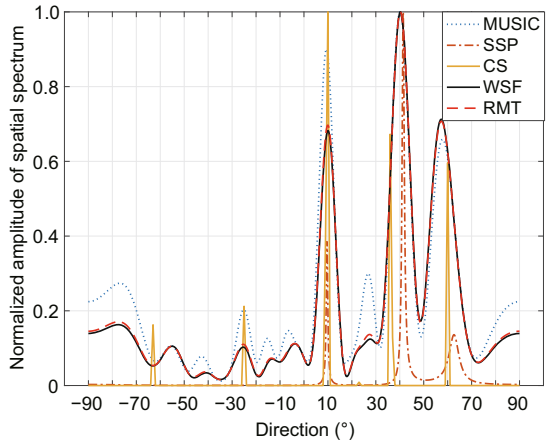

Fig. 2 Normalized amplitude of spatial spectrum versus the search direction ranging from −90° to 90° (SNR: −8 dB; number of snapshots: 10)

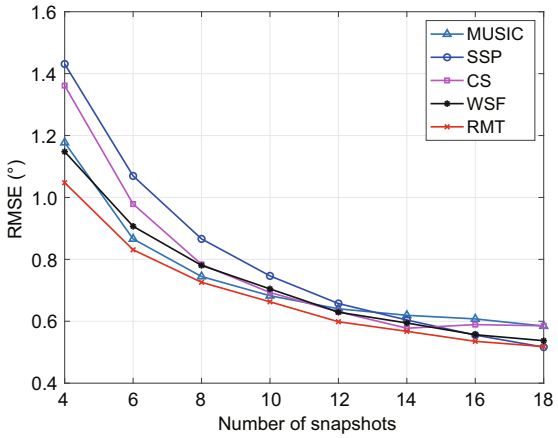

Fig. 4 RMSE versus the number of snapshots varying from 4 to 18 under correlated signals with coefficient 0.8 (SNR: −3 dB)

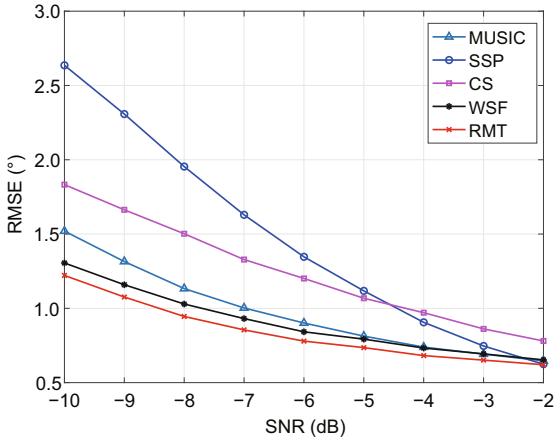

Fig. 3 RMSE versus SNR varying from −10 to −2 dB under correlated signals with coefficient 0.8 (number of snapshots: 10)

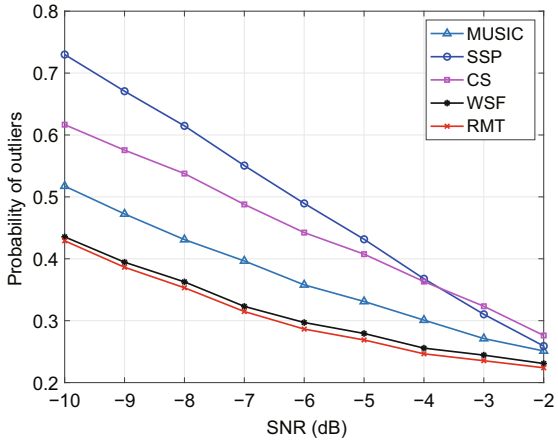

Fig. 5 Probability of outliers versus SNR varying from −10 to −2 dB under correlated signals with coefficient 0.8 (number of snapshots: 10)

over 0.5° are considered as outliers. The estimation error of RMT is lower than the errors computed from MUSIC, SSP, CS, and WSF at few snapshots and a low SNR because of the superiority of RMT in this kind of scenario. The lower error probability of RMT compared with those of MUSIC, SSP, CS, and WSF also verifies its better performance.

Comparative simulations of MUSIC, SSP, CS, WSF, and RMT methods are performed under the third scenario (Figs. 7 and 8). While the signals are uncorrelated, RMSE and the probability of outliers of RMT are still lower than the counterparts of the other methods at a low SNR and small number of snapshots, which also proves the superiority of RMT.

The proposed method is used to deal with signal subspace weighting. For coherent signals, the rank of the signal subspace decreases; thus, our method is unsuitable for DOA estimation of coherent signal sources.

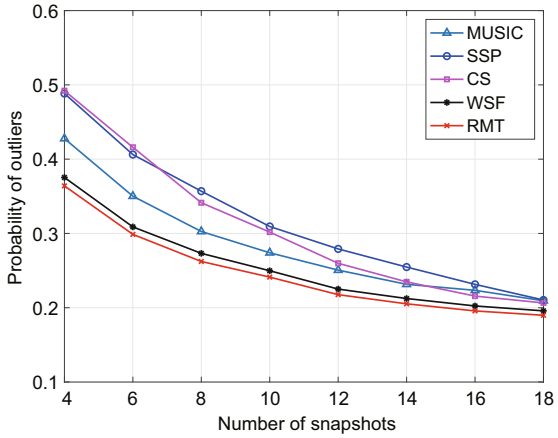

Fig. 6 Probability of outliers versus the number of snapshots varying from 4 to 18 under correlated signals with coefficient 0.8 (SNR: −3 dB)

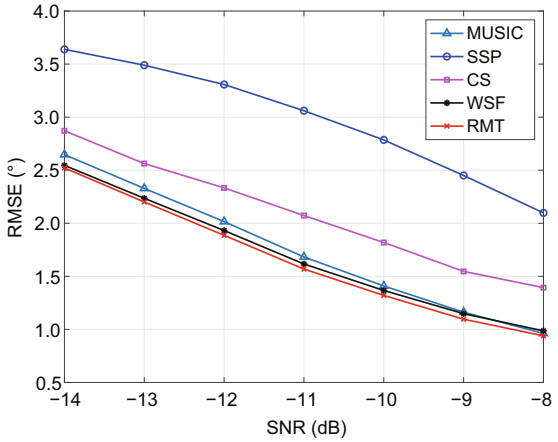

Fig. 7 RMSE versus SNR varying from −14 to −8 dB with uncorrelated signals (number of snapshots: 10)

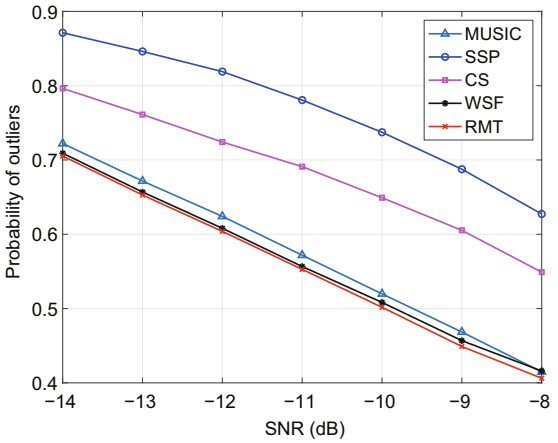

Fig. 8 Probability of outliers versus SNR varying from −14 to −8 dB with uncorrelated signals (number of snapshots: 10)

4 Conclusions

In this paper, we have presented a new method of DOA estimation for narrow-band signals. The weighting matrix is calculated to achieve a lower RMSE. The performance of RMT is better than those of MUSIC, SSP, CS, and WSF under the same scenario with few snapshots and at a low SNR, which was verified through numerical simulations.

Contributors

Ye-chao BAI designed the research. Yu-meng GAO and Ye-chao BAI processed the data. Yu-meng GAO drafted the manuscript. Ye-chao BAI, Jiang-hui LI, and Qiong WANG helped organize the manuscript. Yu-meng GAO, Qiong WANG, and Xing-gan ZHANG revised and finalized the paper.

Compliance with ethics guidelines

Yu-meng GAO, Jiang-hui LI, Ye-chao BAI, Qiong WANG, and Xing-gan ZHANG declare that they have no conflict of interest.

References

Asendorf NA, 2015. Informative Data Fusion: Beyond Canonical Correlation Analysis. PhD Thesis, University of Michigan, State of Michigan, USA.

Bai XJ, Li YA, Zhang W, et al., 2014. Direction of arrival estimation of two wide-band sources with small array based on beam-space coherent signal-subspace method.

In: Xing S, Chen S, Wei Z (Eds.), Unifying Electrical Engineering and Electronics Engineering. Springer, New York, p.1415-1423. https://doi.org/10.1007/978-1-4614-4981-2-155

Bai YC, Li JH, Wu Y, et al., 2018. Weighted incoherent signal subspace method for DOA estimation on wideband colored signals. *IEEE Access*, 7:1224-1233. https://doi.org/10.1109/ACCESS.2018.2886250

Basha TSG, Sridevi PV, Prasad MNG, 2013. Beam forming in smart antenna with precise direction of arrival estimation using improved music. *Wirel Person Commun*, 71(2):1353-1364. https://doi.org/10.1007/s11277-012-0879-9

Benaych-Georges F, Nadakuditi RR, 2011. The eigenvalues and eigenvectors of finite low rank perturbations of large random matrices. *Adv Math*, 227(1):494-521. https://doi.org/10.1016/j.aim.2011.02.007

Chen H, Zhang XG, Wang QS, et al., 2018. Efficient data fusion using random matrix theory. *IEEE Signal Process Lett*, 25(5):605-609. https://doi.org/10.1109/LSP.2018.2815557

He X, Ai Q, Qiu RC, et al., 2017. A big data architecture design for smart grids based on random matrix theory. *IEEE Trans Smart Grid*, 8(2):674-686. https://doi.org/10.1109/TSG.2015.2445828

Krim H, Viberg M, 1996. Two decades of array signal processing research: the parametric approach. *IEEE Signal Process Mag*, 13(4):67-94. https://doi.org/10.1109/79.526899

Li S, He W, Yang XG, et al., 2014. Direction-of-arrival estimation of quasi-stationary signals using two-level Khatri-Rao subspace and four-level nested array. *J Cent South Univ*, 21(7):2743-2750. https://doi.org/10.1007/s11771-014-2236-5

Liu AH, Yang Q, Zhang X, et al., 2018. Modified root music for co-prime linear arrays. *Electron Lett*, 54(15):949-950. https://doi.org/10.1049/el.2018.1125

Schmidt R, 1986. Multiple emitter location and signal parameter estimation. *IEEE Trans Antenn Propag*, 34(3):276-280. https://doi.org/10.1109/TAP.1986.1143830

Viberg M, Ottersten B, Kailath T, 1991. Detection and estimation in sensor arrays using weighted subspace fitting. *IEEE Trans Signal Process*, 39(11):2436-2449. https://doi.org/10.1109/78.97999

Wan LT, Han GJ, Jiang JF, et al., 2017. DOA estimation for coherently distributed sources considering circular and noncircular signals in massive MIMO systems. *IEEE Syst J*, 11(1):41-49. https://doi.org/10.1109/JSYST.2015.2445052

Wu XG, Guo TW, 2011. Direction of arrival parametric estimation and simulation based on MATLAB. Int Conf on Informatics, Cybernetics, and Computer Engineering, p.147-156. https://doi.org/10.1007/978-3-642-25188-7_18

Zhao LM, Liu HQ, Li Y, et al., 2015. DOA estimation under sensor gain and phase uncertainties. Int Conf on Estimation, Detection and Information Fusion, p.209-213. https://doi.org/10.1109/ICEDIF.2015.7280192